Silica Nanohybrid Membranes with High CO2 Affinity for Green Hydrogen Purification

ADVANCED ENERGY MATERIALS
www.advenergymat.de

Materials Views
www.MaterialsViews.com

Silica Nanohybrid Membranes with High CO_2 Affinity for Green Hydrogen Purification

Cher Hon Lau, Songlin Liu, Donald R. Paul, Jianzhong Xia, Yan-Ching Jean, Hongmin Chen, Lu Shao, and Tai-Shung Chung**

An effective separation of CO_2 from H_2 can be achieved using currently known polyethylene oxide (PEO)-based membranes at low temperatures but the CO_2 permeability is inadequate for commerical operations. For commercial-scale CO_2/H_2 separation, CO_2 permeability of these membranes must be significantly enhanced without compromising CO_2/H_2 selectivity. We report here exceptional CO_2/H_2 separation properties of a nanohybrid membrane comprising polyethylene glycol methacrylate (PEGMA) grafts on an organic-inorganic membrane (OIM) consisting of a low molecular weight polypropylene oxide (PPO)-PEO-PPO diamine and 3-glycidyloxypropyltrimethoxysilane (GOTMS), an alkoxysilane. The CO_2 gas permeability of this nanohybrid membrane can reach 1990 Barrer with a CO_2/H_2 selectivity of 11 at 35 °C for a mixed gas mixture comprising 50% CO_2 - 50% H_2 at 3.5 atm. The transformation of the inorganic silica phase from a well-dispersed network of finely defined nanoparticles to rough porous clusters appears to be responsible for this OIM membrane exceeding the performance of other state-of-the-art PEO-based membranes.

1. Introduction

The emergence of H_2 as a green energy has attracted much attention for improving current H_2 production and purification techniques.[1] Industrial H_2 production techniques[2] that are based on the oxidative conversions of hydrocarbons to hydrogen gas (Equation 1) require a subsequent water gas shift (WGS) reaction (Equation 2) to increase H_2 content. In these processes, CO_2 is produced as a byproduct and is traditionally removed using cost- and energy- intensive post-treatment gas separation techniques.[3] Green technologies like membranes[4,5] with high CO_2 permeability and ideal gas separation capabilities[6–9] can overcome the shortcomings of traditional CO_2-separation techniques.

$$C_nH_m + nH_2O + \text{heat} \leftrightarrow nCO + \left(\frac{m}{2} + n\right)H_2 \quad (1)$$

$$CO + H_2O \leftrightarrow CO_2 + H_2 \quad (2)$$

Gas permeability (P) in membranes is governed by the product of solubility (S) and diffusivity (D) coefficients, i.e. $P = S \times D$. Gas separation membranes can be classified as conventional membranes that operate based on gas diffusivity selectivity, i.e., size selection, and reverse-selective membranes that rely on gas solubility selectivity. CO_2/H_2 separation is ideally achieved using reverse-selective membranes that preferentially allow larger CO_2 gas molecules to permeate to low pressures while retaining the smaller H_2 gas molecules in the retentate at high pressures.[5,6,9,10] Most membranes are expected to have $S_{CO2}/S_{H2} > 1$ and $D_{CO2}/D_{H2} < 1$ based on size and thermodynamic differences between CO_2 and H_2; however, reverse-selective membranes have a sufficiently high solubility selectivity that overcomes the adverse diffusivity selectivity. An effective strategy has been to find materials that have a high CO_2 affinity.[6] For instance, in amorphous polyethylene oxide (PEO) membranes, a CO_2/H_2 selectivity of 10 at 35 °C was achieved by enhancing S_{CO2} via a dipole-quadrapole interaction between the acidic CO_2 and the polar ether oxygens.[11] Industrial-scale CO_2/H_2 separation for green hydrogen production by membranes would be more practical if the CO_2 permeability of current state-of-the-art PEO-based membranes are significantly increased while maintaining similar or achieving higher selectivity.

Organic-inorganic membranes (OIMs) synthesized from simple fabrication processes have shown high CO_2 affinity that leads to good CO_2 permeability and CO_2/light gas separation.[12] Sforça, Yoshida, and Nunes first demonstrated that polyether-silica organic-inorganic membranes synthesized using sol-gel

C. H. Lau, Dr. S. Liu, J. Z. Xia, Prof. T.-S. Chung
Department of Chemical & Biomolecular Engineering
National University of Singapore
4 Engineering Drive 4, 117576 Singapore
E-mail: chencts@nus.edu.sg
Prof. D. R. Paul
Department of Chemical Engineering
The University of Texas at Austin
1 University Station C0400, Austin TX 7812-0231, USA
Prof. Y.-C. Jean, Dr. H. Chen
Department of Chemistry
University of Missouri—Kansas City
5100 Rockhill Road, Kansas City, MO 64110, USA
Prof. L. Shao
School of Chemical Engineering and Technology
State Key Laboratory of Urban Water Resource and Environment (SKLUWRE)
Harbin Institute of Technology
150001, PR China
E-mail: shaolu@hit.edu.cn

DOI: 10.1002/aenm.201100195

processes possessed CO_2 permeabilities that could reach 125 Barrer. The H_2 and N_2 permeabilities reached 18 and 2.1 Barrer, respectively. Evidently, the superior CO_2 permeability attributes to high CO_2/N_2 selectivity of 89 and good CO_2/H_2 selectivity of 9. Acid-catalyzed sol-gel methods yield OIMs that possess finely dispersed inorganic nanoparticles in the organic phase.[13,14] In our recent work,[10] we reported that OIMs fabricated using polyether diamines and silica (PEDS) display comparable CO_2/H_2 separation properties to the membranes synthesized from cross-linked organic PEO-acrylate monomers.[6] At 35 °C, the CO_2 permeability of this base PEDS OIM reaches 370 Barrer with a CO_2/H_2 selectivity of 9.[10] At the expense of good mechanical properties, CO_2 permeabilities of these OIMs were enhanced with the addition of more polyether diamines.[10] To enhance CO_2 permeability while inhibiting the side effects of excessive polyether content, we proposed to graft short polyether side-chains onto the OIMs. The addition of PEG side-chains can minimize chain mobility in the main chains, thus, retaining mechanical strengths while enhancing the interaction of the resultant nanohybrid material with highly condensable gas penetrants.

2. Results and Discussion

2.1. Materials Characterization

Following detailed procedures from our previous work,[10] together with wet ozonolysis, CH_x sites in the base PEDS OIM can be converted into peroxide moieties.[15] Subsequently, polyethylene glycol methacrylate (PEGMA with $M_w = 360$) is grafted onto the ozone-modified base PEDS OIM via free radicals, produced by the thermal decomposition of the peroxide moieties, initiating a propagation reaction that increased the side-chain length as shown in **Figure 1**. Unreacted PEGMA was leached

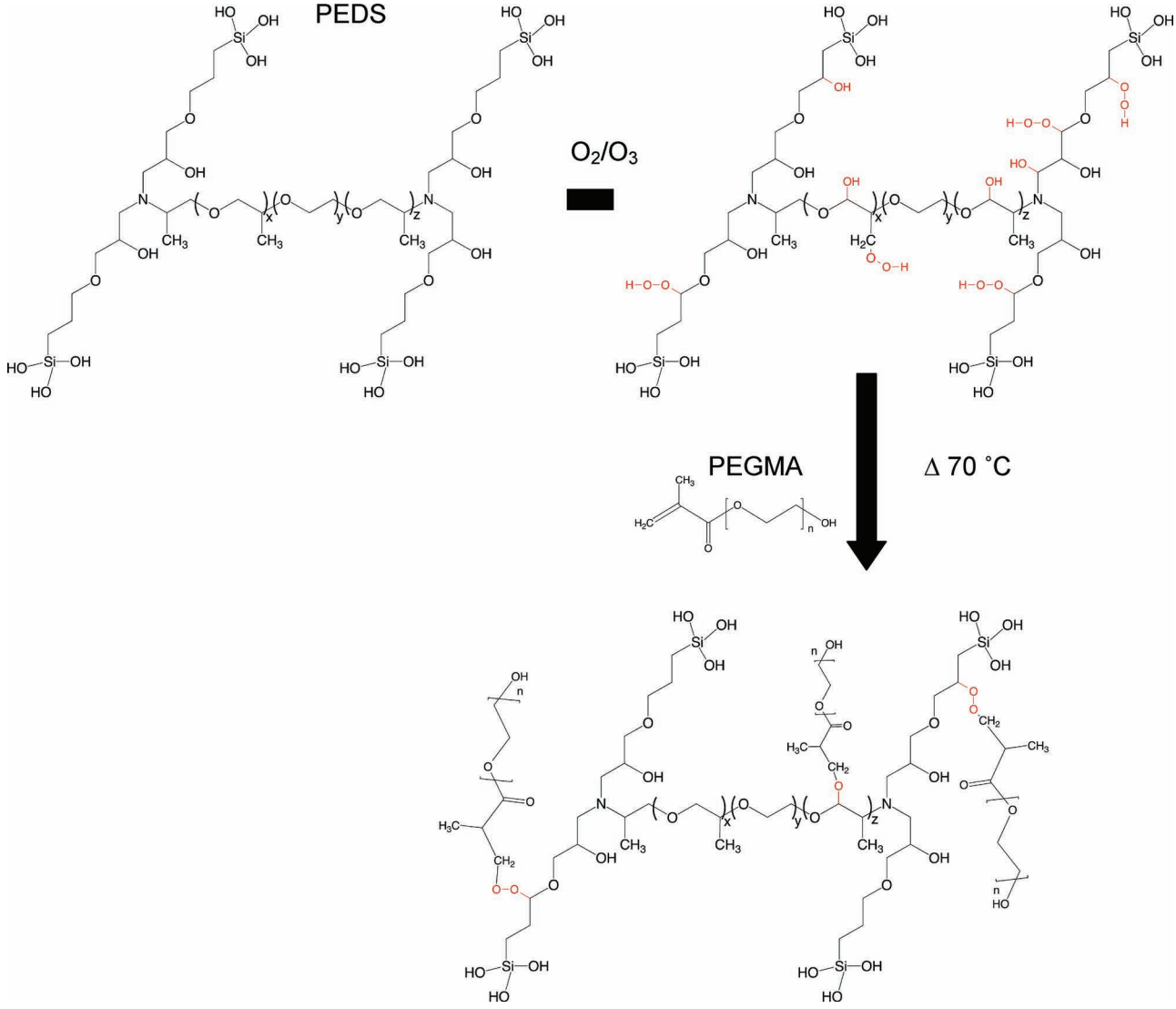

Figure 1. Schematic representation of the PEDS-P20 network. Different lengths of PEGMA grafts can propagate in any direction as the PEDS main chains are in the amorphous phase. The CH_x moieties were converted into COOH or COO^- moieties via wet ozonolysis. Free radicals are formed via thermal decomposition.

from the resultant product that was subsequently dried at 70 °C under vacuum for 24 hours. The PEGMA graft content was determined by comparing the weight of the membranes before and after washing. Results indicate that 11, 15, and 20 wt.% of PEGMA is grafted onto the base materials when 27, 33 and 43 wt.% of PEGMA was initially added to the solution mixture consisting of 80 wt.% PPO-PEO-PPO diamine and 20 wt.% epoxysilane. Throughout this work, by "PEDS-PXX" we refer to OIMs comprising XX wt.% of PEGMA (with respect to the total amount of the base material) grafted onto a PEDS base material comprising 80 wt.% PPO-PEO-PPO diamine and 20 wt.% GOTMS. The ^{13}C NMR spectra in **Figure 2** validate the presence of PEGMA grafts in these nanohybrid membranes. By comparing the ^{13}C NMR spectra of PEDS-P00 (Figure 2a) and PEDS-P20 (Figure 2b) OIMs, peaks belonging to the CH (δ = 55.05 ppm) and CH_3 (δ = 9.58 ppm) moiety of PPO[16] resonate to lower δ values at δ = 54.49 ppm and 8.92 ppm upon ozonolysis and the addition of PEGMA. Additionally, a peak (δ = 51 ppm) correlating to an OCOR terminal group is observed in the ^{13}C NMR spectrum of PEDS-P20 OIM.[16] This ascertains the grafting of PEGMA onto the main PEDS chains. The absence of peaks corresponding to C = C (between δ = 115–140 ppm)[16] indicates that unreacted PEGMA is successfully removed from the nanohybrid membranes. The inorganic networks in all classes of PEDS-based OIMS studied in this work have the same chemical composition as confirmed by

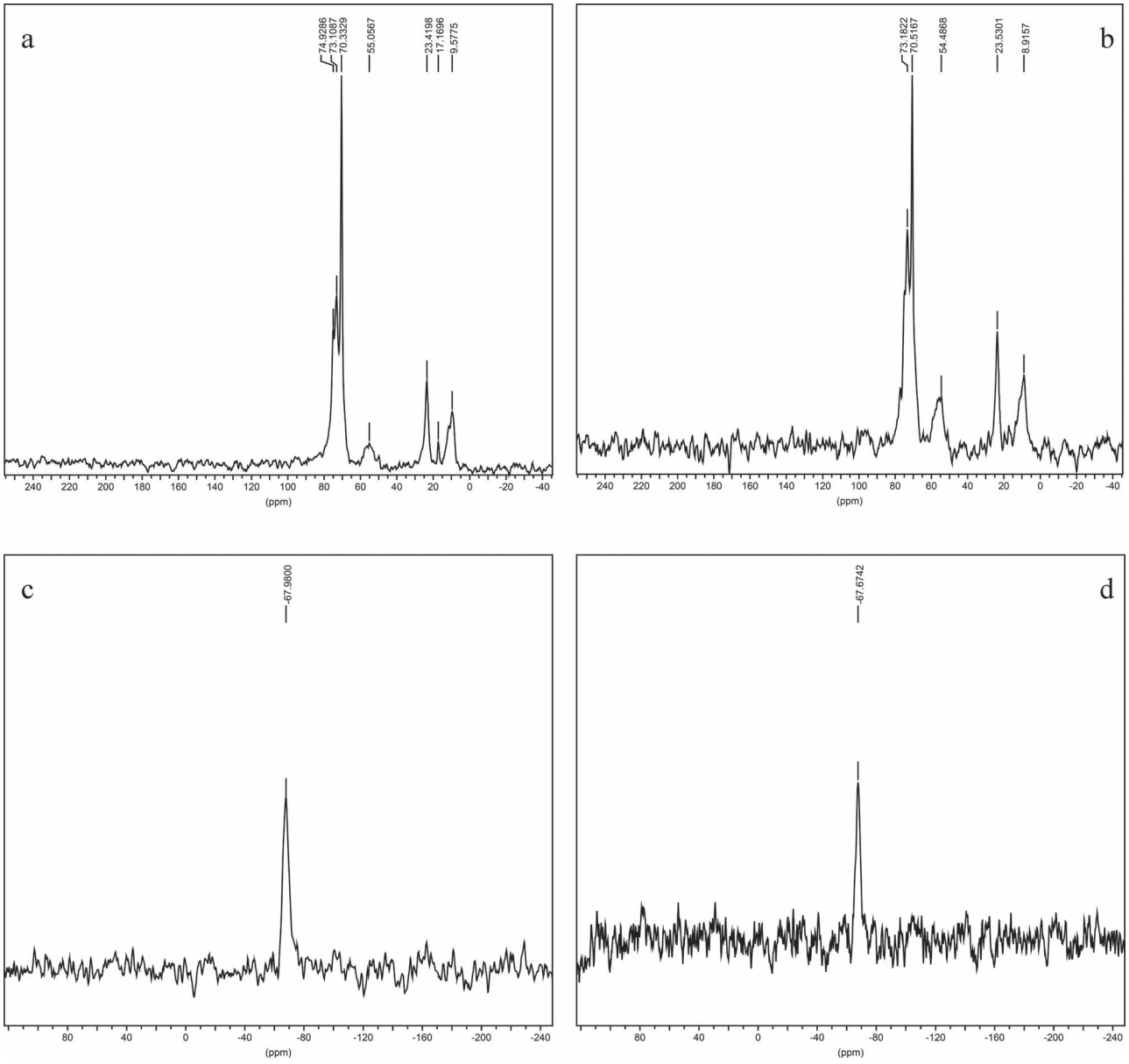

Figure 2. (a) ^{13}C solid state NMR of PEDS-P00 nanohybrid membrane (b) ^{13}C solid state NMR of PEDS-P20 nanohybrid membrane (c) ^{29}Si solid state NMR of PEDS-P00 nanohybrid membrane (d) ^{29}Si solid state NMR of PEDS-P20 nanohybrid membrane.

^{29}Si solid-state NMR. The ^{29}Si NM R spectra of PEDS-P00 and PEDS-P20 OIMs show a peak (δ = 67 ppm) that correlates to T^3 resonances arising from fully condensed silicons, indicating complete condensation of GOTMS.[12,13]

The free volume (V_f) and relative fractional free volume (FFV) contents of PEDS-PXX OIMs are elucidated using positron annihilation lifetime spectroscopy (PALS). The V_f radii size distribution correlates to the lifetime (τ_3 in ns) of ortho-positroniums (*o*-Ps) while *o*-Ps intensity (I_3 in%) correlates to *o*-Ps formation i.e. V_f content.[17–19] The V_f radii distributions of PEDS-P00, PEDS-P15, and PEDS-P20 nanohybrid membranes are shown in **Figure 3**. Compared to PEDS-P00 membranes, all PEGMA-grafted nanohybrid membranes display higher FFV content. PEGMA grafts of up to 15 wt.% increase I_3 and τ_3 values of PEDS-based OIMs while 20 wt.% of PEGMA grafts cause I_3 and τ_3 values of PEDS-based OIMs to decrease. Using the I_3 and τ_3 values, the relative free fractional volume (FFV) of these OIMs are estimated by $AV_f I_3$, whereby A is an empirical constant and $V_f = 4\ \pi R^3/3$.[18] The penetrant diffusion coefficient of a material increases as a function of FFV content. A linear relationship between CO_2 pressure (up to 20 atm) and FFV content indicate that CO_2 sorption in PEDS-P00 and PEDS-P20 OIMs obey Henry's law, whereby CO_2 sorption occurs via the swelling of existing free volume or the creation of new CO_2 sorption sites. The trends observed in I_3 and τ_3 values as a function of PEGMA content are observed in the FFV contents of PEDS-P00 and PEDS-P20 OIMs. In PEDS-P20 OIMs, longer hydroxyl (OH)-terminated PEGMA chains increase the tendency to form hydrogen bonds with neighboring ether moieties in PEDS main-chains or PEGMA side-chains, thus further reducing chain mobility that consequently reduces free volume content.[19] As the aforementioned PALS data are obtained at room temperature, it is important to elucidate the FFV of these nanohybrid membranes at 35 °C (testing temperature). Figure 3(c) shows that FFV content decreases as a function of temperature decrements. Additionally, Figure 3(c) shows that the FFV content in PEDS-P20 membranes is lower than that of PEDS-15 membranes. Although FFV content in PEDS-P20 membranes is lower than that of PEDS-P15 membranes; the CO_2 permeability of a PEDS-P20 nanohybrid membrane is the highest amongst other PEGMA-grafted PEDS nanohybrid membranes. This is attributed to the higher S_{CO2} coefficient observed in the PEDS-20 nanohybrid membranes. The effects of solubility coefficients on gas permeability are explained in a latter section.

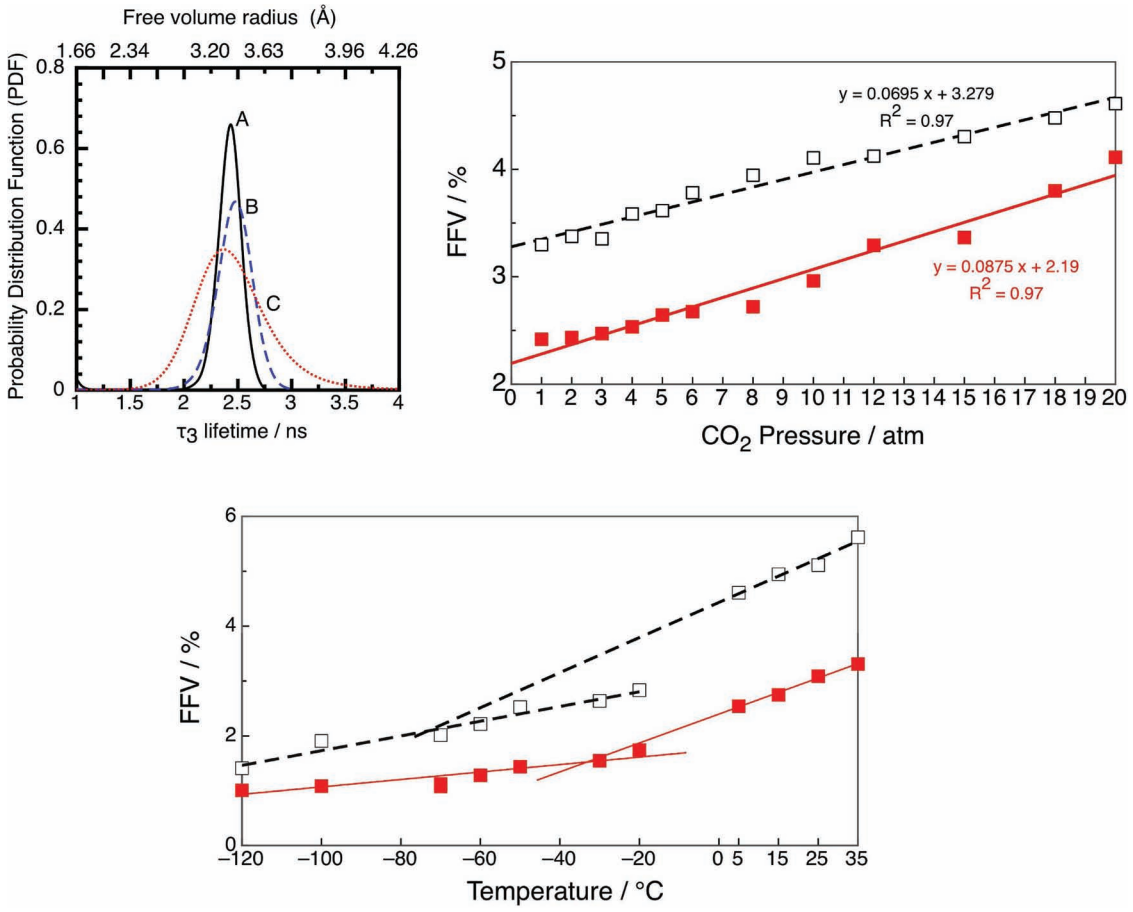

Figure 3. (a) Distribution of free volume radius in PEDS-based OIMs grafted with different PEGMA content. A–PEDS-P00 (black), B–PEDS-P15 (blue), and C–PEDS-P20 (red). (b) FFV content of PEDS-P00 (solid), and PEDS-P20 (empty) OIMs at different CO_2 pressures. (c) FFV content of PEDS-P00 (solid), and PEDS-P20 (empty) OIMs at different temperatures.

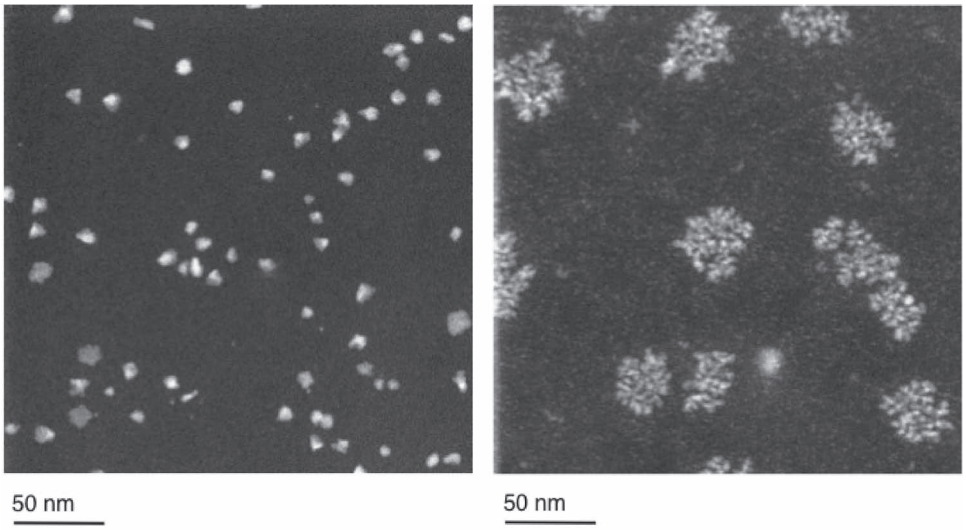

Figure 4. STEM images of (a) PEDS-P00 OIM and (b) PEDS-P20 OIM. Si-based nanostructures with good edge definition are observed in PEDS-P00 OIMs while rough edged Si-based nanostructures can be observed in PEDS-P20 OIMs.

Scanning transmission electron spectroscopy (STEM) images of PEDS-P00 and PEDS-P20 OIMs in **Figure 4** reveal finely dispersed inorganic phases in the organic polyether phases. EDX analyses indicate that these nanoparticles are primarily made up of silicon and oxygen. The well-defined silica nanoparticles in PEDS-P00 OIMs range from 5–10 nm in diameter sizes while bigger silica nanostructures ranging from 40–100 nm are observed in PEDS-P20 OIMs. The size increment in Si-based nanostructures ascribes to the change in H_2O/Si ratio (R-ratio) in the sol-gel process during synthesis.[20] Unreacted PEGMA additives in the synthesis solution of PEDS-P20 OIM can form hydrogen bonds with water, thus reducing the R-ratio value that subsequently induces roughness in the larger inorganic nanoparticles.[20] It is important to note that additional PEGMA causes only structural changes to the inorganic network while maintaining chemical composition integrity, as evidenced by ^{29}Si solid-state NMR (Figure 2(c) and (d)). The amount of non-colloidal or "unseen" silicon in PEDS-P00 and PEDS-P20 OIMs is determined by comparing the area occupied by the silica in Figure 4. As the R-ratio decreases, rough silica clusters are formed (evident in Figure 4) to reduce surface energy. The surface energy of these clusters are thermodynamically favored and lower when compared to smaller nanoparticles (Ostwald ripening effect),[20] thus less energy is required to facilitate CO_2 desorption, hence increasing CO_2 permeability. Calculations using the M_w of -Si-$(O)_3$ show that there are 29.3 and 51.3 wt.% of non-colloidal Si in PEDS-P00 and PEDS-P20 OIMs, respectively. A large presence of non-colloidal Si in these OIMs yields free siloxane bonds. Consequently, these free siloxane bonds behave like CO_2 sorption sites and further enhances CO_2 affinity in these organic-inorganic membranes.[21]

It is a well-known fact that amorphous PEO-based materials generally possess high CO_2 permeabilities. DSC data (not shown here) have proved that the melting temperatures (T_m) of these PEDS nanohybrid materials are below the testing temperature of 35 °C. Hence these materials are amorphous during gas permeation. **Figure 5** shows that the pure gas CO_2 and H_2 permeabilities of the PEDS-P20 nanohybrid membrane can reach 1,950 Barrer and 185 Barrer, respectively, with an ideal CO_2/H_2 selectivity of 11. Compared to PEDS-P00 membranes, ideal CO_2 and H_2 permeability coefficients are augmented by 5.2 and 4.7 fold, respectively. The larger increment in ideal CO_2 permeability causes the CO_2/H_2 selectivity to increase from 8.9 to 10.9. Compared to highly amorphous PEO-based CO_2 selective membranes,[6,8,22] the nanohybrid membranes studied in this work possess better CO_2 transport properties with lower EO content. This indicates that contributions of the inorganic silica phase are more significant than the organic polyether phase. Pure gas CO_2 permeability subtly increases with increasing CO_2 pressure (from 2 to 20 atm) and displays no sign of plasticization. Plasticization takes place when polymer chain segmental mobility is increased via the sorption of the gas penetrant i.e. CO_2.[23] The presence of PEGMA side chains and silica nanoparticles possibly hinder main chain mobility in these organic-inorganic materials. Thus, even when CO_2 is sorbed in these materials, chain segmental mobility is hardly affected and plasticization is minimal. At 3.5 atm, the effects of plasticization are negligible in these nanohybrid membranes. The mixed gas permeation properties of these nanohybrid membranes are determined using different mixed gases comprising 50 mol.% CO_2: 50 mol.% H_2, 60 mol.% CO_2: 40 mol.% H_2, and 90 mol.% CO_2: 10 mol.% H_2. The CO_2 permeability of a PEDS-P20 nanohybrid membrane can reach 1990 Barrer with a CO_2/H_2 selectivity of 11. The mixed and ideal gas permeation tests results are identical. While the CO_2 transport and separation properties in our nanohybrid membranes have not surpassed the upper bound limit for CO_2/H_2 separation,[24] these nanohybrid membranes represent a tremendous improvement from current state-of-the-art membranes. Besides larger FFV content, the significant gas separation performance observed in alkyl methacrylate grafted OIMs can be ascribed to the crucial enhancement in CO_2 solubility coefficients caused by the CO_2- affinity of the inorganic silicate phases.

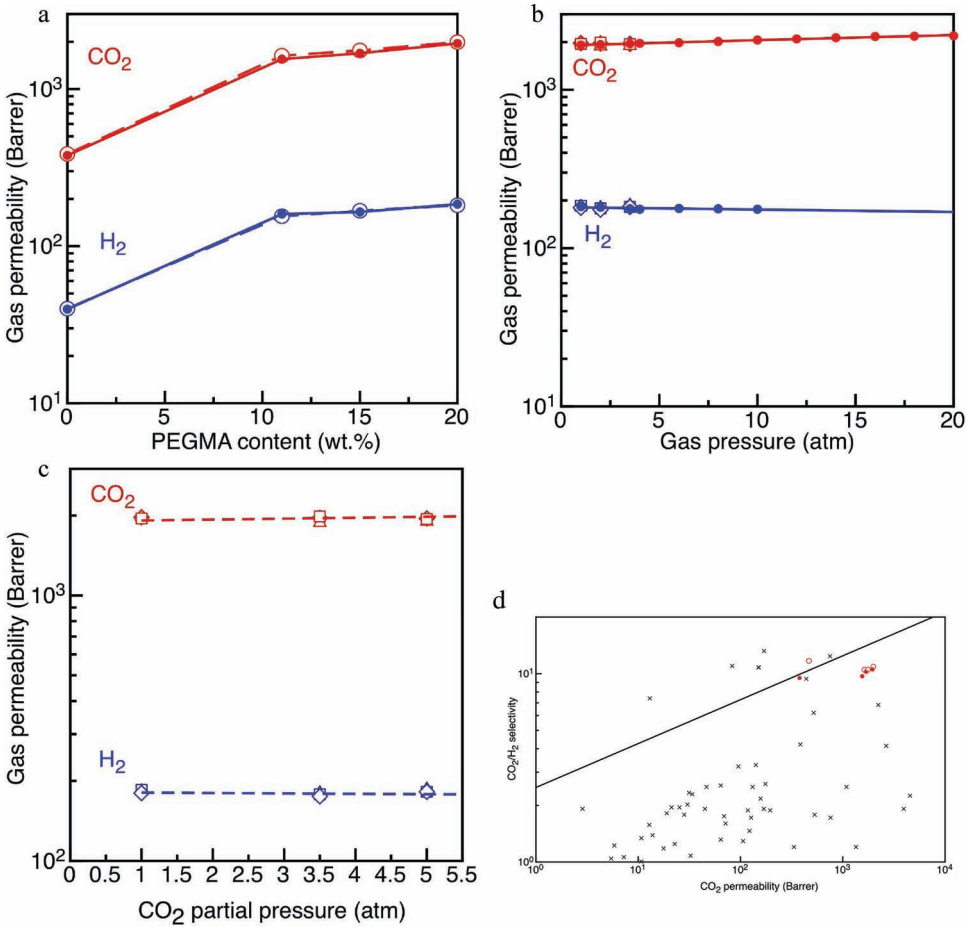

Figure 5. (a) Comparison between pure gas permeabilities (•–CO_2, •- H_2) and mixed gas permeabilities (■- CO_2, ■- H_2) of PEGMA-grafted PEDS OIMs with different PEGMA graft content. All gas permeation tests are tested at 35 °C, while pure gas pressures and CO_2 partial pressures are maintained at 3.5 atm. (b) A comparison of pure gas permeabilities and mixed gas permeabilities of PEDS-P20 nanohybrid membrane at different gas pressures. (c) The effects of 1, 3.5 and 5 atm of CO_2 partial pressures using mixed gases with different feed compositions. Mixed gas feed compositions (CO_2 mol.%: H_2 mol.%) are represented by □(50:50), △(60:40), and □(90:10). For safety purposes, the maximum H_2 pressure is maintained at 10 atm. Uncertainty in permeability measurements is ±10%. The lines are provided to guide the eye. (d) Pure (CO_2 and H_2) and mixed gas permeabilities of PEDS-P20 OIM membranes tested at 35 °C and 3.5 atm. • and ■ represent CO_2 permeabilities obtained from pure and mixed gas tests, respectively. **x** shows the CO_2/H_2 separation performances of other membranes.[6] In these samples, PEGMA concentration ranged from 0 wt.% to 20 wt.%. The line represents the revised upper bound limit by Robeson that correlates gas permeability to selectivity.[24]

The concentration of alkyl methacrylate added during synthesis strongly influences the CO_2 solubility (S_{CO2}) and diffusivity (D_{CO2}) coefficients of these nanohybrid membranes. CO_2 solubility coefficients calculated from sorption isotherms of PEDS-based nanohybrid membranes shown in **Figure 6** indicate that S_{CO2} increases as a function of PEGMA content. **Table 1** shows that the activation energy of CO_2 permeation $(E_P)_{CO2}$ decreases as the content of PEGMA increases. It can be argued as follows that the trends in S_{CO2} and in $(E_P)_{CO2}$ are related. The activation energy for permeation is the sum of the activation energy of diffusion and the enthalpy of sorption of the gas in the polymer; the latter consists of the enthalpy of condensation of the gas plus the enthalpy of mixing gas and polymer. Increasing the content of units with good CO_2 affinity i.e. EO units and siloxane units enhances the interaction of CO_2 with the polymer; this means a more negative heat of mixing of CO_2 with the polymer and, thus, a lower activation energy of permeation for CO_2.

Interestingly, the sorption isotherms of PEDS-P00 and PEDS-P20 nanohybrid membranes closely resemble the sorption isotherms of polydimethylsiloxane (PDMS) and poly (1-trimethylsilyl-1-propyne) (PTMSP), respectively. The solubility coefficients of PEDS-based nanohybrid membranes can be described as a summation of all the contributions of individual components; namely, the amorphous polyether (organic phase), the silica inorganic network, and the amorphous PEGMA grafts. Based on the composition of PPO-PEO-PPO diamines (80 wt.%) and epoxysilanes (20 wt.%) in PEDS-P00 nanohybrid membranes, the theoretical S_{CO2} coefficient may be calculated using the solubility coefficients of amorphous PEO (A-PEO),[25] PDMS,[26] PTMSP,[27] and the following equation:

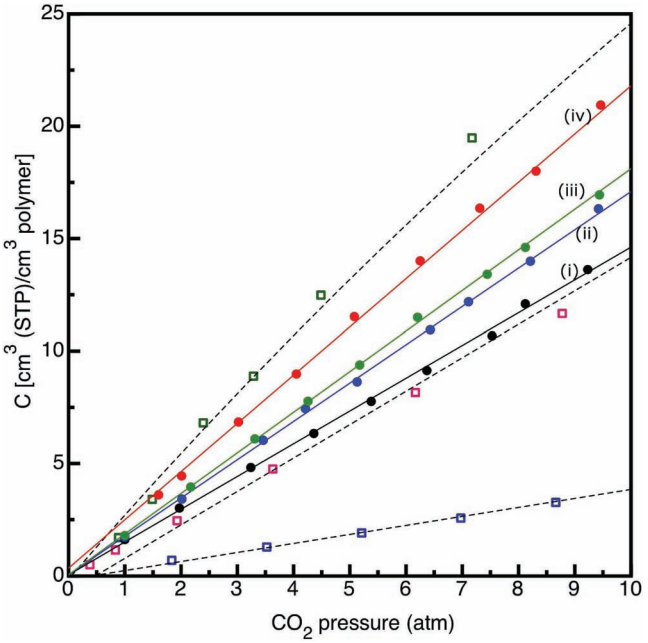

Figure 6. The CO_2 sorption isotherms of (i) PEDS-P00 (•), (ii) PEDS-P11 (•), (iii) PEDS-P15 (•), and (iv) PEDS-P20 (•). The solid dots represent experimental data while the empty dots refer to theoretical S_{CO2} coefficients of ■–amorphous PEO,[25] ■–PDMS,[26] and ■–PTMSP.[27] Solubility coefficients are measured in cm^3(STP)/cm^3 polymer atm.

S_{CO2} of PEDS-PXX = (1–x) [0.8 (S_{CO2} A-PEO) + 0.2 (S_{CO2} PDMS or PTMSP)] + x (S_{CO2} A-PEO) whereby x = amount of grafted PEGMA

The theoretical (1.54 cm^3.STP/cm^3.atm) and experimental S_{CO2} coefficients of the PEDS-P00 nanohybrid membrane (1.5 cm^3.STP/cm^3.atm) are very close when the S_{CO2} coefficient of PDMS is used. The inorganic phase of a PEDS-P00 nanohybrid membrane behaves like a PDMS network that consists of Si-O bonds. The high CO_2 affinity of Si-O bonds[21] that are present in PEDS-P00 nanohybrid membranes yields a higher S_{CO2} coefficient when compared to amorphous, cross-linked rubbers.[19] In the case of PEDS-P11 and PEDS-P15 nanohybrid membranes, the identical experimental and theoretical S_{CO2} coefficients also indicate that the inorganic networks in these nanohybrid membranes possess PDMS-like CO_2 sorption capabilities. In the case of a PEDS-P20 nanohybrid membrane, the calculated theoretical S_{CO2} coefficient is very close to the experimental value when the CO_2 solubility coefficient of PTMSP[27] is used. As S_{CO2} of PTMSP is larger than the S_{CO2} of PDMS, the P_{CO2} PEDS-P20 is larger than that observed in PEDS-P15 membranes. The difference in solubility contributions is due to structural differences (caused by different R-ratios in the sol-gel processes) in the silica-based networks that affect the interaction between CO_2 penetrant and CO_2-philic moieties like Si-O moieties and ether oxygen units. Based on these observations, we concur that the increment in P_{CO2} in PEDS-P20 membranes can be attributed to significant increments in S_{CO2} while the increment in P_{CO2} in PEDS-P15 or PEDS-P10 membranes are primarily ascribed to significant increments in D_{CO2}.

3. Conclusions

CO_2 permeability and CO_2/H_2 selectivity enhancements in PEGMA-grafted PEDS OIMs can be ascribed to markedly improved D_{CO2} and S_{CO2} coefficients. The presence of non-reactive additives in the pre-synthesis mixture solutions induced structural changes in the inorganic phases. The ultra-high CO_2 permeability and gas selectivity of these nanohybrid membranes render this material exceptionally effective in facilitating a low-cost, clean technique for industrial-scale H_2 purification while performing CO_2 capture. Moreover, preliminary studies indicate that the CO_2/H_2 selectivity of these nanohybrid membranes is further enhanced in the presence of water vapor. The effects of water vapor on these nanohybrid membranes will be studied in future work. Large-scale utilization of this material for CO_2/H_2 separation can positively contribute huge economical savings based on the elimination of H_2 recompression. Moreover, these OIMs are able to effectively purify H_2 from syngas feeds that contain up to 50% CO_2. Additionally, the low N_2 permeability (35 Barrer) of PEDS-P20 materials indicates that these materials can also be used for CO_2 removal in flue gas i.e. the CO_2/N_2 selectivity of PEDS-P20 is 55.7.

Table 1. Ideal CO_2 permeability, solubility and diffusivity coefficients of PEDS-based OIMs, amorphous cross-linked PEO rubbers[25], PDMS[26], and PTMSP.[27] Diffusivity coefficients are measured in cm^2/s.

Sample code	P_{CO2} (Barrer)	S_{CO2} (cm^3 STP/ cm^3. atm)	D_{CO2} (10^{-6} cm^2/s)	$E_{P\,CO2}$ (kJ/mol)	$\alpha_{CO2/H2}$	I_3 (%)	τ_3 (ns)	FFV content (%)
PEDS-P00	378	1.5	1.92	22.4 ± 0.28	9.5	12.7	2.59	3.2
PEDS-P11	1550	1.7	6.92	13.4 ± 0.45	9.69	-	-	-
PEDS-P15	1690	1.8	7.14	11.9 ± 0.32	10.24	16.2	2.65	4.8
PEDS-P20	1950	2.3	6.44	10.5 ± 0.22	10.54	12.7	2.45	3.6
Semi-crystalline PEO[25]	300	1.6	1.43	21–23.45	9.4	-	-	-
PDMS[26]	3800	1.3	22.21	-	3.1	-	-	-
PTMSP[27]	28000	3.9	54.56	-	1.3	-	-	-

4. Experimental Section

Materials and membrane preparation: The polypropylene oxide–polyethylene oxide–polypropylene oxide (PPO-PEO-PPO) diamine, (M_w = 2000 g/mole), polyethylene glycol methacrylate (PEGMA: M_w=360 g/mole), ethanol (HPLC grade) and 3-glycidyloxypropyltrimethoxysilane (GOTMS: M_w = 236 g/mole) were purchased from Sigma Aldrich, Singapore. Hydrochloric acid (HCl) was purchased from Fisher Scientific. All chemicals and solvents, except for PEGMA, were used as received. The inhibitors in PEGMA were removed using activated carbon. For every 100 mL of PEGMA, 4 g of activated carbon was added and stirred for 1 h, after which, the activated carbon was filtered from this mixture. These procedures were repeated 3 times. The purified PEGMA was stored at 4 °C.

A catalyzing aqueous solution containing 37.5 wt.% HCl was used to hydrolyze GOTMS. After 30 min of hydrolysis at room temperature, the alkoxysilane solution was immediately added to a solution consisting of 2 wt.% polyether diamine dissolved in 70 wt.% ethanol and 30 wt.% distilled water. An epoxy-amine reaction was facilitated by stirring the resultant organic-inorganic solution at 750 rpm at 60 °C for one hour. The organic-inorganic solution was allowed to cool to room temperature prior to 60 s of wet ozonolysis. Wet ozonolysis was carried out using an AC Faradayozone–high concentration ozone generator (L10G). High purity oxygen (contained in a 10 L cylinder) obtained from SOXAL, Singapore was converted into ozone (ozone flow was limited to 0.5 litres per minute). After wet ozonolysis, PEGMA was added to the ozonolyzed mixture and the resultant solution was stirred at 70 °C for 24 hours to facilitate PEGMA grafting.

Organic-inorganic polyether diamine-epoxysilane-PEGMA membranes were fabricated using a slow-casting method. After transferring the solution into a Teflon dish, the solvent was evaporated at 30 °C for 24 h. Subsequently, the temperature was raised to 40 °C for further evaporation. Nascent films were peeled off and dried at 70 °C for 24 h to remove residual solvent whilst undergoing full condensation. Prior to characterization, all membranes were immersed in deionized water for 5 days to remove unreacted monomers. The deionized water was changed everyday. The weight difference between the washed membranes and as-cast membranes is about 16–23 wt.%. Based on calculations and the wt.% of materials used, a mole of polyether diamine will react with 2 moles of alkoxysilanes. Hence, we can assume that nearly all of the alkoxysilanes reacted with the polyether diamines and the weight loss in washed membranes can be attributed to unreacted PEGMA. These nanohybrid membranes were stored in a dry box with 27% humidity at 25 °C prior to testing and characterization.

Membrane characterization: The chemical structures of the PEDS-based OIM membranes were characterized using solid-state ^{29}Si and ^{13}C NMR. The ^{29}Si (79.5 MHz) and ^{13}C (100.6 MHz) NMR with magic angle spinning (MAS) at 7.5 kHz was performed with a Bruker DRX 400 spectrometer. Samples were ground using a freeze miller prior to analysis. Scanning-transmission electron microscopy (STEM) was used to observe the silica morphology and dispersion. To prepare samples for STEM characterization, solutions containing nanohybrid materials were diluted from 2-wt% to 0.01 wt-%. The high-angle annular dark field scanning-TEM (HAADF-STEM) studies and EDX analysis were carried out using a FEI Titan 80-300 electron microscope equipped with an electron beam monochromator, an energy dispersive X-ray spectroscopy (EDX) and a Gatan electron energy loss spectrometer. The accelerating voltage of the electron beam was 200 KeV. The scanning electron beam size of EDX measurement was around 0.3 nm. To prepare the nanohybrid samples for positron annihilation lifetime (PAL) characterization, a positron source (15 μCi ^{22}NaCl purchased from DuPont Pharmaceutical Division, Delaware) was sandwiched between two pieces of membrane (10 mm × 10 mm × ~1 mm) and then sealed between two 12 μm thick Kapton films. The assembled samples were exposed to different temperatures and CO_2 pressures in a specially designed set-up. The CO_2 pressure in this set-up was monitored using an Omega transducer pressure gauge (Model 302-1KGY). The positron annihilation lifetime (PAL) spectra were recorded using a fast-fast coincident PAL spectrometer (resolution = 280 ps) at the University of Missouri-Kansas City. The acquired PAL spectra (1 million counts) were analyzed into 3-mean lifetimes and into lifetime distributions using PATFIT and MELT computer programs. The longest lifetime from these analyses (τ_3 in ns) is due to the pick off annihilation of ortho-positroniums (*o*-Ps) in free volume cavities (V_f). The V_f mean radius and volume were tabulated using well-established semi-empirical equations based on the spherical infinite potential-well model.[28] The fractional free volume (FFV) of these nanohybrid materials is shown as a product of τ_3 (ns) and I_3 (%). For the V_f radius size distribution, only results calculated from *o*-Ps lifetime distribution from MELT analysis were reported.

The pure gas permeabilities were determined by a constant volume-variable pressure method. The gas permeabilities of H_2 and CO_2 at 3.5 atm were determined from the steady-state rate of downstream pressure build-up rate (dp/dt) via Equation 3:

$$P = D \times S = \frac{273 \times 10^{10}}{760} \frac{VL}{AT\left[\frac{p_2 \times 76}{14.7}\right]} \left(\frac{dp}{dt}\right) \quad (3)$$

where P is the permeability of a membrane to a gas and its unit is in Barrer (1 Barrer = 7.5005 m^2 s^{-1} Pa^{-1}, SI units), D is the average effective diffusivity (cm^2/s), S is the apparent sorption coefficient/solubility (cm^3 (STP)/cm^3 polymer cmHg), V is the volume of the downstream chamber (cm^3), L is the film thickness (cm). A refers to the effective area of the membrane (cm^2), T is the experimental temperature (K) and the pressure of the feed gas in the upstream chamber is given by p_2 (psia). In water vapor-saturated ideal gas permeation tests, the gas bubbles through water prior to feeding. The relative humidity of the permeating gas is detected using a Vaisala HMT330 transmitter and calculated using the Vaisala Veriteg vLog software. Relative gas humidity is about 90%.

The ideal separation factor of a membrane for gas A to gas B, which is the product of diffusivity selectivity and solubility selectivity, was evaluated as follows:

$$\alpha_{A/B} = \frac{P_A}{P_B} = \frac{S_A}{S_B} \times \frac{D_A}{D_B} \quad (4)$$

A mixed gas mixture containing x-mol.% of H_2 in CO_2 was used as the feed gas mixtures and the measurements were conducted at 35 °C with a CO_2 partial pressure of 3.5 atm. The molar concentrations of H_2 tested in this work are 50 mol.%, 40 mol.%, and 10 mol.%. To ensure constant gas molarity in the retentate, small amounts of retentate are slowly discharged into water or the atmosphere via a silicon piping. The sampling process was initiated by evacuating the line from the receiving volume (the lower chamber: downstream) to GC by vacuum pump. The compositions of the feed and permeate were analyzed by GC. The choice of carrier gas in the GC setup is nitrogen. Similar to the pure gas permeability, the mixed gas steady state permeation rate were then determined by following equations:

$$P_{H_2} = \frac{273 \times 10^{10}}{760} \frac{(1 - y_{CO_2})VL}{AT(76/14.7)[(1 - x_{CO_2})p_2]} \times \left(\frac{dp_1}{dt}\right) \quad (5)$$

$$P_{CO_2} = \frac{273 \times 10^{10}}{760} \frac{y_{CO_2}VL}{AT(76/14.7)(x_{CO_2}p_2)} \times \left(\frac{dp_1}{dt}\right) \quad (6)$$

where P_{CO2} and P_{H2} are, respectively, the gas permeability of CO_2 and H_2 (Barrer), p_2 is the upstream feed gas pressure (psia), p_1 is the downstream permeate gas pressure (psia), x_{CO2} is the mole fraction of CO_2 in the feed gas (%)and y_{CO2} is the mole fraction of CO_2 in the permeate (%), V is the volume of the downstream chamber (cm^3), L is the film thickness (cm). Subsequently, the separation factor for mixed gas permeation can be simplified to Equation (4) due to the negligible downstream pressure.

Carbon dioxide sorption tests were conducted using a Cahn D200 microbalance sorption cell at 35 °C over a pressure range of 0–250 psi (0–17.24 bar). A detailed description of the dual volume sorption cell was reported elsewhere.[29] For each sample, films with thickness of 300 μm, sides of 1 cm, and total mass of approximately 80-100 mg were placed on the sample pan. The system was evacuated for 24 h prior to testing. The gas at a specific pressure was fed into the system. The mass of gas sorbed by the membranes at equilibrium was recorded. Subsequent sorption experiments were done by further increment of the gas pressure. The equilibrium sorption values obtained were corrected for buoyancy effects. CO_2 solubility coefficients of each sample were obtained from the slope of the sorption isotherms. Subsequently, CO_2 diffusivity coefficients were calculated using Equation (3).

Acknowledgements

The authors would like to thank the Singapore National Research Foundation (NRF) for support through the Competitive Research Program for the project entitled, "Molecular engineering of membrane materials: research and technology for energy development of hydrogen, natural gas and syngas" (grant number R-279-000-261-281). The authors express their appreciations to Dr. Xiao Youchang, Dr. Li Yi and Ms. Chua Meiling and Ms. Wang Huan for their assistance and valuable suggestions during this work. The authors would also like to thank Dr. Lin Ming and Miss Joyce Tan from the Institute of Materials Research and Engineering (IMRE), A*STAR for the help rendered in STEM characterizations.

Received: April 9, 2011
Revised: May 22, 2011
Published online: June 14, 2011

[1] R. F. Service, *Science* **2004**, *305*, 958.
[2] N. Z. Muradov, in *Hydrogen fuel: production, transport and storage*, (Ed: R. B. Gupta), CRC Press, Boca Raton, FL **2009**.
[3] R. Trygve, F. H. Elisabet, J. S. V. Preben, U. Øystein, in *Hydrogen Production and Storage: R&D Priorities and Gaps*, International Energy Agency, **2006**.
[4] L. Shao, B. T. Low, T. S. Chung, A. R. Greenberg, *J. Membrane Sci.* **2009**, *327*, 18.
[5] R. W. Baker, *Ind. Eng. Chem. Res.* **2002**, *41*, 1393.
[6] H. Lin, E. Van Wagner, B. D. Freeman, L. G. Toy, R. P. Gupta, *Science* **2006**, *311*, 639.
[7] a) N. P. Patel, A. C. Miller, R. J. Spontak, *Adv. Mater.* **2003**, *15*, 729; b) N. P. Patel, A. C. Miller, R. J. Spontak, *Adv. Funct. Mater.* **2004**, *14*, 699; c) W. Yave, A. Szymczyk, N. Yave, Z. Roslaniec, *J. Membrane Sci.* **2010**, *362*, 407.
[8] W. Yave, A. Car, S. S. Funari, S. P. Nunes, K.-V. Peinemann, *Macromolecules* **2009**, *43*, 326.
[9] T. C. Merkel, B. D. Freeman, R. J. Spontak, Z. He, I. Pinnau, P. Meakin, A. J. Hill, *Science* **2002**, *296*, 519.
[10] L. Shao, T. S. Chung, *Int. J. Hydrogen Energy* **2009**, *34*, 6492.
[11] a) H. Lin, B. D. Freeman, *J. Membrane Sci.* **2004**, *239*, 105; b) H. Lin, B. D. Freeman, *J. Mol. Struct.* **2005**, *739*, 57.
[12] M. L. Sforça, I. V. P. Yoshida, S. P. Nunes, *J. Membrane Sci.* **1999**, *159*, 197.
[13] P. Hajji, L. David, J. F. Gerard, J. P. Pascault, G. Vigier, *J. Polym. Sci. Part B: Polym. Phys.* **1999**, *37*, 3172.
[14] S. Yano, K. Iwata, K. Kurita, *Mater. Sci. Eng. C* **1998**, *6*, 75.
[15] Y. Chen, L. Ying, W. Yu, E. T. Kang, K. G. Neoh, *Macromolecules* **2003**, *36*, 9451.
[16] R. M. Silverstein, F. X. Webster, D. J. Kiemle, *Spectrometric Identification of organic compounds*, John Wiley & Sons, Hoboken, NJ **2005**.
[17] H. B. Park, C. H. Jung, Y. M. Lee, A. J. Hill, S. J. Pas, S. T. Mudie, E. Van Wagner, B. D. Freeman, D. J. Cookson, *Science* **2007**, *318*, 254.
[18] H. Chen, M.-L. Cheng, Y. C. Jean, L. J. Lee, J. Yang, *J. Polym. Sci. Part B: Polym. Phys.* **2008**, *46*, 388.
[19] H. Lin, E. V. Wagner, J. S. Swinnea, B. D. Freeman, S. J. Pas, A. J. Hill, S. Kalakkunnath, D. S. Kalika, *J. Membrane Sci.* **2006**, *276*, 145.
[20] C. J. Brinker, *J. Non-Cryst. Solids* **1988**, *100*, 31.
[21] V. M. Shah, B. J. Hardy, S. A. Stern, *J. Polym. Sci. Part B: Polym. Phys.* **1986**, *24*, 2033.
[22] a) A. Car, C. Stropnik, W. Yave, K.-V. Peinemann, *Adv. Funct. Mater.* **2008**, *18*, 2815; b) A. Car, C. Stropnik, W. Yave, K.-V. Peinemann, *Separation Purification Technol.* **2008**, *62*, 110.
[23] S. R. Reijerkerk, K. Nijmeijer, C. P. Ribeiro Jr., B. D. Freeman, M. Wessling, *J. Membrane Sci.* **2011**, *367*, 33.
[24] L. M. Robeson, *J. Membrane Sci.* **2008**, *320*, 390.
[25] H. Lin, B. D. Freeman, *Macromolecules* **2006**, *39*, 3568.
[26] T. C. Merkel, V. I. Bondar, K. Nagai, B. D. Freeman, I. Pinnau, *J. Polym. Sci. Part B: Polym. Phys.* **2000**, *38*, 415.
[27] V. Bondar, A. Alentiev, T. Masuda, Y. Yampolskii, *Macromol. Chem. Phys.* **1997**, *198*, 1701.
[28] a) M. Eldrup, D. Lightbody, J. N. Sherwood, *Chem. Phys.* **1981**, *63*, 51; b) S. J. Tao, *J. Chem. Phys.* **1971**, *56*, 5499.
[29] R. Wang, C. Cao, T. S. Chung, *J. Membrane Sci.* **2002**, *198*, 259.